River detection in high-resolution SAR data using the Frangi filter and shearlet features

Yuhan Liu, Lingbing Peng, Suqi Huang, Xiaoyang Wang, Yuqing Wang & Zhenming Peng

Published online: 07 Jul 2019.

Submit your article to this journal ⬈

Article views: 38

View Crossmark data ⬈

Taylor & Francis
Taylor & Francis Group

Check for updates

River detection in high-resolution SAR data using the Frangi filter and shearlet features

Yuhan Liu [a], Lingbing Peng[a], Suqi Huang[a], Xiaoyang Wang[b], Yuqing Wang[c] and Zhenming Peng[a]

[a]School of Information and Communication Engineering, University of Electronic Science and Technology of China, Chengdu, China; [b]Department of Electrical & Electronic Engineering, University of Bristol, Bristol, UK; [c]Changchun Institute of Optics, Fine Mechanics and Physics, Chinese Academy of Science, Changchun, China

ABSTRACT

River extraction plays an important role in several applications such as monitoring and navigation, and synthetic aperture radar (SAR) is one of the major sensors of remote sensing. This paper proposes an algorithm to detect a river from high-resolution SAR images mainly based on the Frangi filter and shearlet features with the help of an active contour model (ACM). The Frangi filter is firstly applied to enhance the river and then the shearlet features are computed by the shearlet transform. A rule of feature selection is then proposed to acquire the corresponding features of the river. Finally, binarization and an active contour model are implemented to extract the river. The approach is tested on SAR images and the experimental results demonstrate that the proposed method is effective.

1. Introduction

River extraction from remote sensing images is of great significance to water monitoring, ship navigation and so on (Gao et al. 2017; Klemenjak, Waske, and Valero et al. 2012). In recent years, synthetic aperture radar (SAR) images have become increasingly important in the field of remote sensing because information can be collected around the clock and in all weather conditions (Sun and Mao, 2011).

Several methods have been developed to detect rivers. The most commonly utilized approaches are based on region growth, wavelet edge information and thresholding with the help of an active contour model (ACM) such as Sun and Mao (2011), Niedermeier, Romaneeßen, and Lehner (2000, 2001), Zhang, Zhang, and Wang et al. (2009) and Wang et al. (2015) extracted the river by wavelet. Niedermeier et al., Lin and Tong (2008) and Wang et al. (2011) recognized rivers with edge extraction. Moreover, Dillabaugh, Niemann, and Richardson (2002), Niedermeier et al., Wang et al. (2015) and Li, Wang, and Liu et al. (2014) applied active contour model to river detection. From the review, we can see that the majority of approaches utilized active contour model and

---

achieved good performance. However, using edge information are easily confused by other scenes like buildings, bridges and wavelet features without direction information has limited ability for complex scenes. Other methods are mainly based on supervised classification algorithms. Klemenjak, Waske, and Valero et al. (2012) proposed an automatic selection of training samples and morphological profiles to detect a river from TerraSAR-X images. Tian et al. (2012) fused corner features and support vector machine (SVM) for river detection. However, the classification methods are limited for practical applications because they require large numbers of samples for training and learning, which is time-consuming (Gao et al. 2017).

From the above, it is clear that a pre-processing step must be applied (M O, Foucher, and Lepage 2016) and an active contour model is an effective method for river extraction. Inspired by linear or strip feature enhancement in medical images, we propose to employ a Frangi filter (Frangi et al. 1998) for pre-processing. Furthermore, wavelet-based methods do not involve directionality of the river. Considering that river responses are high in some directions and other background elements such as buildings or farmland perform similarly in various directions, we compute shearlet decomposition to acquire multiscale and multidirectional features of SAR images. After selecting appropriate shearlet features of the river, thresholding and an active contour model are employed to extract the river. The novel aspects of our proposed algorithm are threefold: 1) Utilizing the Frangi filter to pre-process the SAR images to enhance the region of the river; 2) Making use of directionality of the river by shearlet transform; 3) Designing a feature selection method to acquire the features of the river.

2. Methodology

2.1. Framework of the proposed algorithm

The proposed method mainly consists of four steps: 1) Pre-processing the SAR image by Frangi filter; 2) Acquiring shearlet features of the pre-processed image in different directions and scales; 3) Selecting the appropriate features; 4) Thresholding and utilizing an active contour model with the help of removing interferences to detect the river. The flowchart of our approach is depicted in Figure 1.

2.2. Pre-processing

As the length of a river is much greater than its width (Sun and Mao, 2011) and thus the shape of the river appears strip-like, we introduce the Frangi filter, which is utilized for vessel enhancement in medical images, for pre-processing the image. Although this was an intuition, the results demonstrate that this idea works well.
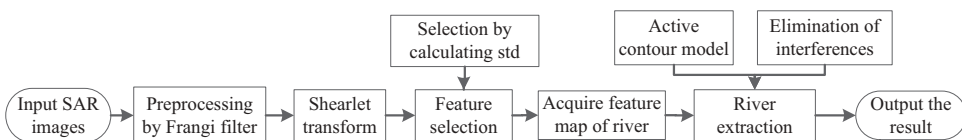
Figure 1. Flowchart of the proposed algorithm.

The gradients of an image express pixel value variation, and second-order derivatives indicate gradient variation. Second-order derivatives are also named the Hessian matrix. Each pixel in the image has a Hessian matrix and each Hessian matrix has two eigenvalues. These eigenvalues describe the degree of change of the pixel value along the corresponding eigenvectors (Frangi et al. 1998). If the pixel has a strip-like structure, the two eigenvalues will be different. Otherwise, the eigenvalues will be similar. Therefore, to enhance the strip and suppress other elements, a discriminative function is proposed, as Frangi et al. described (1998):

$$V_o(\sigma) = \begin{cases} 0 & \text{if } \lambda_2 > 0 \\ \exp\left(-\frac{R^2}{2\beta^2}\right)\left(1 - \exp\left(-\frac{S_B^2}{2c^2}\right)\right) & \text{otherwise} \end{cases} \tag{1}$$

where $V_o(\sigma)$ refers to the response of different standard variation σ in the Gaussian filter used to reduce noise before calculation, and β and c are the threshold values for discrimination, which are set by users and we set them to 0.1 and 20 separately in this work. λ_1 and λ_2 represents the eigenvalue and $\lambda_2 > 0$ for the black background. If the background is white, the condition should be $\lambda_2 < 0$. $R = \lambda_1/\lambda_2$ is a judge function of the strip and $S_B = \sqrt{\lambda_1^2 + \lambda_2^2}$ is a judge function of the background. Here, $|\lambda_1| < |\lambda_2|$ and the final response is the maximum response between the different σ and we consider $\sigma \in [1, 8]$ in this paper.

2.3. Shearlet features

Shearlet transform is one of the multiscale geometric analysis (MGA) methods that can analyze a signal in different scales and directions (Labate, Lim, and Kutyniok et al. 2005). Furthermore, shearlet transform can be computed in the frequency domain and thus the computation is fast. In this work, we utilize fast finite shearlet transform (FFST, Häuser and Steidl 2014) and it is calculated as follows:

$$\psi_{j,k}(\mathbf{x}) = \psi(\mathbf{A}_j^{-1}\mathbf{S}_{j,k}^{-1}(\mathbf{x} - \mathbf{t})) \tag{2}$$

where $\mathbf{x}$ is signal and $\mathbf{A}_j = \begin{bmatrix} 1/4^j & 0 \\ 0 & 1/2^j \end{bmatrix}$ is a scale parameter to separate the image into different scales, $\mathbf{S}_{j,k} = \begin{bmatrix} 1 & k/2^j \\ 0 & 1 \end{bmatrix}$ is a directional parameter to acquire various directional responses, and $\mathbf{t}$ is a translation. j represents the scales and k represents the directions. ψ represents shearlet transform. Thus, we can analyze our image in different scales and directions. We set $j = 2$ and $k = 8$ in this work and thus we can acquire a low-frequency scale and a high-frequency scale with 8 directions at each scale.

2.4. Feature selection

In this section, we describe a rule to select the accurate features of the river in each scale and thus, both low-frequency information and high-frequency details can be preserved. From the above we can make two assumptions: 1) If the directions of the shearlet features and the river are the same, the river will be more obvious and different than other pixels; 2) If the directions of the shearlet features and the river are not consistent, all pixels will

respond similarly. Therefore, we propose two further assumptions: 1) For the features whose shearlet directions are the same as the river, their standard deviations (sd) are higher because there exist apparently different pixels (river); 2) For the features whose shearlet directions are not the same as the river, their standard deviations are lower because the response of all the pixels is the same. Thus, we first normalize the features and then compute the standard deviations of all shearlet features as

$$SF_{j,k} = (SH_{j,k} - \min(SH_{j,k}))/(\max(SH_{j,k}) - \min(SH_{j,k})) \tag{3}$$

$$\boldsymbol{d}(n) = \mathrm{std}(SF_{j,k}) \; n = 1, 2, ...j \times k \tag{4}$$

where SH presents the original shearlet features and SF is the normalized shearlet features, j represents the scales and k is the directions, which are 2 and 8 in this article. $\boldsymbol{d}$ is a vector for all of the standard deviations and n is the index. std means calculating standard deviations. Finally, we find the maximum two sd from $\boldsymbol{d}$ and select the features corresponding to the index of these sd at each scale, which means four features are chosen in total. If we only select one feature with the maximum sd for each scale, some information may be lost and thus we select two features to preserve the river and suppress other elements as much as possible. After the feature selection, we acquire a final feature map of the river by simple summation of the corresponding selected four features and this final feature map will be processed later.

2.5. Image segmentation and river extraction

The final feature map enhances the river and thus we should utilize a relatively high value to segment the image to preserve the river and eliminate other elements. Thus, we consider the mean value added with standard deviation. Moreover, in order to increase the robustness of our algorithm, we propose to segment the feature map with an adaptive threshold T which is calculated as

$$T = \mu + a \times \sigma \tag{5}$$

where μ is the mean value and σ is standard deviation of the feature map. a is an empirical value and is set to 5 in this paper. Although this is an experimental value, it works well in the following tests.

Finally, an active contour model (Chan and Vese 2001) and elimination of disturbing pixels are employed to extract the river in the SAR data with a binary mask that specifies the initial state of the contour. We remove the regions as described by Sun and Mao (2011) with the criteria that the river must be a connecting area, have greater length and have a relatively fixed width that is much smaller than its length. Another is low and evenly distributed grey values in the connecting region.

3. Experimental results

In this section, we first describe the experimental data and evaluations used for the experiments. The experimental results of the proposed approach and comparisons with another method on high-resolution SAR images are then demonstrated. Finally, we discuss the limitations of the proposed method.

3.1. Description of the data

We evaluate the proposed method on two SAR images collected in August 2016 by GF3 satellite. The first one is an image of Beijing airport, China and the resolution is 5 m. The second one is an image of Tianjin, China and the resolution is 10 m. Because there are only two scenes, we divide them into eight blocks containing a region with a river. Six of them are displayed as experimental results and the rest are used for discussion. Furthermore, we create the ground truth manually with a tool called LabelMe (Russell et al., 2008).

3.2. Evaluations

In this work, we use accuracy, recall, precision and kappa coefficients to measure the performance of our method. Accuracy, recall and precision in this context are defined as follows:

$$Accuracy = \frac{area\ of\ detected\ true\ region}{total\ area\ of\ the\ image} \tag{6}$$

$$Recall = \frac{area\ of\ detected\ true\ river}{total\ area\ of\ true\ river} \tag{7}$$

$$Precision = \frac{area\ of\ detected\ true\ river}{total\ area\ of\ detected\ region} \tag{8}$$

3.3. Experiments and results

We first set $\beta = 0.1$, $c = 20$ in the Frangi filter and $j = 2$, $k = 8$ in the shearlet transform. Furthermore, we compare our method with the approach by Yang, et al. (2015) which applies a Gabor filter and path openings and the corresponding parameters are set the same. Moreover, we also compared with the algorithm that first utilizes wavelet to acquire edge information and then applies active contour model with the improvement method same as the proposed. The experimental results of the testing data are shown in Figure 2.

Figure 2 demonstrates that these algorithms for river extraction are effective and can detect most of the river. However, methods all maintain false targets and lose true targets such as in scene 1 and 6. As can be seen in 2, 3 and 4, these approaches all perform well. However, the proposed method achieves superior performance for complex scene in scene 6. From scene 1 we can see that our algorithm and Yang's method perform fairly similarly which means the methods are not robust for different scenes. Furthermore, for scene 7 and 8, our approach and wavelet method achieve similar results. The evaluations of the algorithms are listed in Table 1.

Table 1 presents the measures and we can see that our approach achieves competitive performance, especially in recall and kappa coefficient. These algorithms show equivalent results for accuracy and Yang's method achieves better performance on precision. Furthermore, our algorithm achieves competitive result in the wavelet-based method and
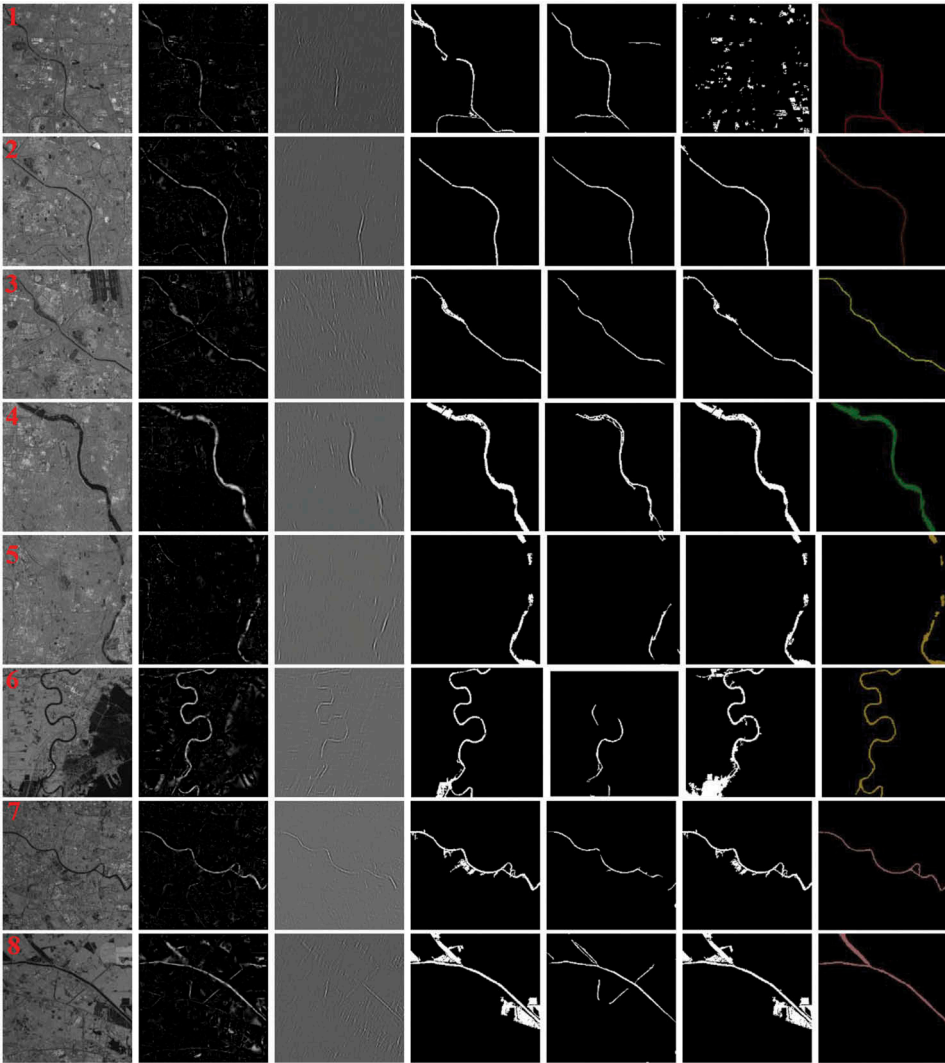
Figure 2. Experimental results for scenes 1 to 8 (column from left to right: original image, filtered image, feature map, the proposed method, Yang's approach, wavelet-based method, ground truth).

is better for complex situation such as 1 and 6. Moreover, we computed the time of these methods: Yang's method needs 0.9 s and wavelet-based approach consumes 1.6 s while the proposed method spends 2.5 s. The time-consuming is slightly low compared with others.

3.4. Discussion

As the results demonstrate, the proposed algorithm does not perform well for all scenes because there are several parameters: β, c, j, k and αneed to be set which may not be appropriate for different images. Although we set them empirically in the experiments, the method still needs to be improved. In this section, we test on scene 1 and discuss

Table 1. Evaluations by proposed and compared method[*].

Scene	Methods	Accuracy	Precision	Recall	Kappa coefficient
1	Proposed	0.9883	0.6678	0.7596	0.7048
	Yang's	0.9888	0.7596	0.6021	0.6661
	Wavelet-based	Failed	Failed	Failed	Failed
2	Proposed	0.9965	0.8958	0.8505	0.8708
	Yang's	0.9953	0.9713	0.6903	0.8047
	Wavelet-based	0.9963	0.8454	0.9054	0.8725
3	Proposed	0.9918	0.6766	0.8381	0.7446
	Yang's	0.9934	0.9542	0.5699	0.7105
	Wavelet-based	0.9928	0.7255	0.8086	0.7611
4	Proposed	0.9937	0.9608	0.9106	0.9317
	Yang's	0.9723	0.9826	0.4509	0.6058
	Wavelet-based	0.9942	0.9589	0.9232	0.9377
5	Proposed	0.9955	0.8317	0.9373	0.8791
	Yang's	0.9874	0.8521	0.3658	0.5065
	Wavelet-based	0.9945	0.7913	0.9407	0.8568
6	Proposed	0.9858	0.7249	0.8614	0.7800
	Yang's	0.9775	0.8917	0.2968	0.4368
	Wavelet-based	0.9513	0.3686	0.8398	0.4908
7	Proposed	0.9862	0.5394	0.9524	0.6822
	Yang's	0.9916	0.9022	0.5362	0.6687
	Wavelet-based	0.9876	0.5669	0.9486	0.7037
8	Proposed	0.9532	0.3732	0.9591	0.5177
	Yang's	0.9811	0.7356	0.5207	0.6004
	Wavelet-based	0.9537	0.3758	0.9548	0.5198

[*]red means that the proposed method is better, blue means Yang's is better and green means wavelet is better
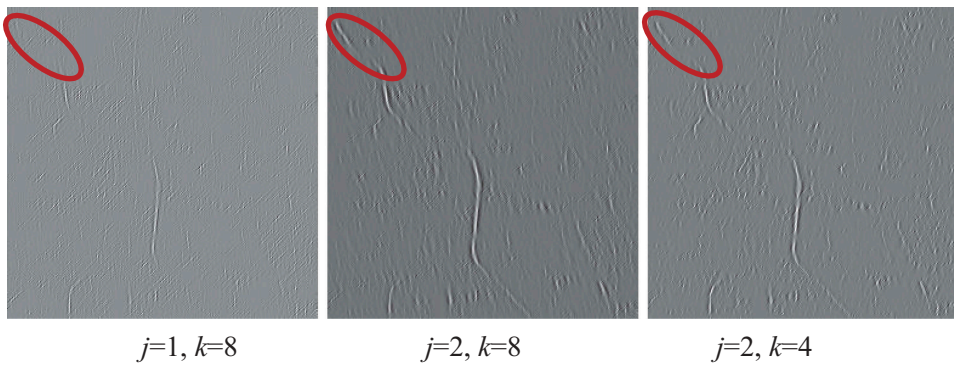
the impact of these parameters. In addition to the parameter to be discussed, others will be same as previous experiments.

3.4.1. Impact of β and c

We tested different β and c and show their performance of enhancement in Figure 3 From Figure 3 we can see if the β is too small or c is too large, the river will not be improved completely while if the β is too large or c is too small, some background may be enhanced as well. Therefore, an appropriate value should be selected.

$\beta = 0.01$ $\beta = 0.05$ $\beta = 0.1$ $\beta = 0.5$ $\beta = 2$

$c=10$ $c=15$ $c=20$ $c=30$ $c=50$
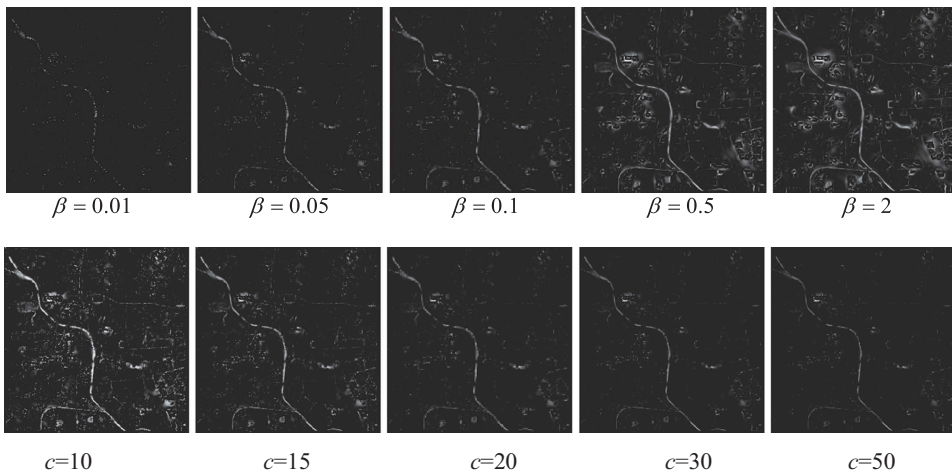
Figure 3. Performance of different β and c on scene 1.

| *j*=1, *k*=8 | *j*=2, *k*=8 | *j*=2, *k*=4 |

Figure 4. Different shearlet features for various scale *j* and direction *k* (circles show the comparison of the performance on preserving the river).

3.4.2. Impact of *j* and *k*

To find the influence of scales and directions in shearlet transform, we computed the fusion features by various scales and directions with the same feature selection strategy described in this work and the results are demonstrated in Figure 4.

Figure 4 shows that to preserve the river better, we should select several scales with directions. If the image is only considered in few directions and one scales, the information will be lost (shown in circle).

3.4.3. Impact of *α*

We tested on scene 1 and changed *a* from 1 to 10. A high threshold will preserve fewer regions and thus reduce the false alarm rate. Meanwhile, the recall will decline because some true river may be eliminated by a high threshold. We plot the variation curves of four measures in Figure 5. Figure 5 illustrates that recall decreases and precision increases as we expected. Moreover, the segmentation does not affect the accuracy and kappa coefficient
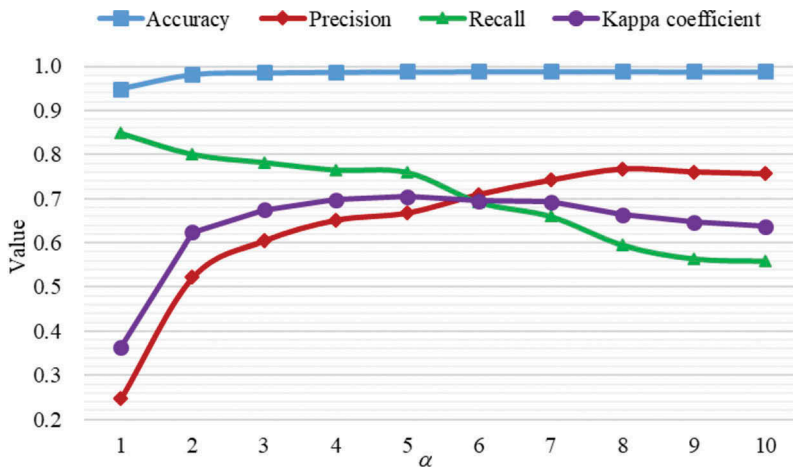
Figure 5. Performance of different *a*.

performs like a quadratic function with a Therefore, an improved T is necessary to balance the measures and to derive optimal results and our algorithm needs improvement.

Although we discuss the impact of corresponding parameters in the proposed algorithm, more specifically, these parameters should be determined adaptively according to the characteristics of river images in our future work.

4. Conclusions

In this paper, we propose an algorithm for river extraction which can efficiently enhance and detect rivers in SAR data. The approach combines the Frangi filter, shearlet features and an active contour model to detect rivers with a feature selection strategy. Experiments performed on images showed good performance. However, there are some defects in our technique such as parameter setting and the robustness, which can be improved in future work.

Acknowledgements

Funding

ORCID

Yuhan Liu http://orcid.org/0000-0003-4328-6427

References

Chan, T. F., and L. A. Vese. 2001. "Active Contours without Edges." *IEEE Transactions on Image Processing* 10: 266–277. doi:10.1109/83.902291.

Demetrio Labate, WangQ Lim, Gitta Kutyniok and Guido Weiss, 2005. "Sparse Multidimensional Representation Using Shearlets". Optics and Photonics 2005, San Diego, California, United StatesWavelets XI. Proceedings of the SPIE, **5914**, pp:254–262.

Dillabaugh, R. C., Niemann, K and Richardson, E. D.. 2002. Semi-Automated Extraction of Rivers from Digital Imagery. *GeoInformatica*. **6**. pp. 263-284. doi: 10.1023/A:1019718019825.

Frangi, A.F., Niessen, W.J., Vincken, K.L. and Viergever, M.A. 1998. "Multiscale vessel enhancement filtering". International Conference on Medical Image Computing and Computer-Assisted Intervention, Springer-Verlag, Lecture Notes in Computer Science. **1496**, Berlin, Germany, pp. 130-137.

Gao, F., Ma, F., Wang, J., Sun, J. P., Yang, E. F., and Zhou, H. Y. 2017. "Visual Saliency Modeling for River Detection in High-resolution SAR Imagery." *IEEE Access* 5:1000–1014.

Häuser, S., and G. Steidl 2014. "Fast Finite Shearlet Transform: A Tutorial." *ArXiv*. https://arxiv.org/pdf/1202.1773.pdf

Klemenjak, S., Waske, B., Valero, S., and Chanussot, J 2012. "Automatic Detection of Rivers in High-Resolution SAR Data". *IEEE Journal of Selected Topics in Applied Earth Observations & Remote Sensing* 5: 1364–1372. doi:10.1109/JSTARS.2012.2189099.

Li, N., Wang. R., Liu, Y., Du, K., Chen, J., and Deng, Y. 2014. "Robust River Boundaries Extraction of Dammed Lakes in Mountain Areas after Wenchuan Earthquake from High Resolution SAR Images Combining Local Connectivity and ACM". *ISPRS Journal of Photogrammetry and Remote Sensing* 94: 91–101. doi:10.1016/j.isprsjprs.2014.04.020.

Lin, Y., L. Yan, and Q. X. Tong 2008. "Automatic Recognition of Rivers from LIDAR Data by Profile Factor". *The International Archives of the Photogrammetry, Remote Sensing and Spatial Information Sciences*. XXXVII Part B1. Beijing.

M. O. Sghaier, S. Foucher and R. Lepage. 2016. "River Extraction from High-Resolution SAR Images Combining a Structural Feature Set and Mathematical Morphology." *IEEE Journal of Selected Topics in Applied Earth Observations and Remote Sensing* 10: 1025–1038.

Niedermeier, A., S. Lehner, and J. V. D. Sanden 2001. "Monitoring Big River Estuaries Using SAR Images" *IEEE International Geoscience and Remote Sensing Symposium, IGARSS*, Sydney, NSW, Australia**4**, pp. 1756–1758.

Niedermeier, A., E. Romaneeßen, and S. Lehner. 2000. "Coastlines in SAR Images Using Edge Detection by Wavelet Methods." *IEEE Transactions on Geoscience & Remote Sensing* 38: 2270–2281. doi:10.1109/36.868884.

Russell, B., A. Torralba, K. Murphy, and W. T. FreemanL. 2008. "LabelMe: A Database and Web-based Tool for Image Annotation." *International Journal of Computer Vision* 77: 157–173. doi:10.1007/s11263-007-0090-8.

Sun, J. P., and Mao, S. Y. 2011. "River Detection Algorithm in SAR Images Based on Edge Extraction and Ridge Tracing Techniques." *International Journal of Remote Sensing* 32: 3485–3494. doi:10.1080/01431161003749477.

Tian, Z., C. Wu, D. Chen, X. Yu, and L. Wang. 2012. "A Novel Method of River Detection for High Resolution Remote Sensing Image Based on Corner Feature and SVM." In Proceeding International Conference Advances in Neural Networks, Lecture Notes in Computer Science, Lecture Notes in Computer Science, Springer, Berlin, Heidelberg **7368**. pp. 266–273.

Wang, W. G., Wang, J., Zhao, H., and Yuan, Y. N. 2015. "River Detection from SAR Images."IEEE 5th Asia-Pacific Conference on Synthetic Aperture Radar (APSAR), Singapore, Singapore, pp.680-683, doi: 10.1109/APSAR.2015.7306297

Wang. X. L., Li. C. S., and Wu, R. B.2011. "River Boundaries Extraction in Mountain Areas for SAR Images with Fusing GIS Information" *IEEE Cie International Conference on Radar*, IEEE. ChengDu, China, pp. 1586–1588.

Yang, K., Li, M., Liu, Y., Cheng, L., Huang, Q., and Chen, Y.2015. "River Detection in Remotely Sensed Imagery Using Gabor Filtering and Path Opening". *Remote Sensing* 7: 8779–8802. doi:10.3390/rs70708779.

Zhang, L., Zhang, Y., Wang, M., and Li, Y 2009. "Adaptive River Segmentation in SAR Images". *Journal of Electronics (china)* 26: 438–442. doi:10.1007/s11767-007-0113-1.